Hybrid modeling of time-dependent rarefied gas expansion

Manuel Vargas, Steryios Naris, and Dimitris Valougeorgis[a)]
Department of Mechanical Engineering, University of Thessaly, Pedion Areos, 38334 Volos, Greece

Sarantis Pantazis and Karl Jousten
Physikalisch-Technische Bundesanstalt, Abbestr. 2-12, 10587 Berlin, Germany

(Received 18 August 2013; accepted 31 October 2013; published 20 November 2013)

The time evolution of the flow parameters in a system where gas is expanded from a high pressure chamber through a tube toward a low pressure chamber is investigated. During the process, the pressure in the two chambers is changing in the opposite direction, while the flow rate is reduced until the system reaches its equilibrium state. Rarefied conditions may be present. Based on the observation that the characteristic time in the chambers is several orders of magnitude larger than that in the tube, the evolution of the flow is modeled in a hybrid manner. At each time step, based on kinetic theory, a steady-state flow configuration is solved to estimate the amount of gas passing through the tube (micromodel) and then the pressure of the two vessels is updated by applying the mass conservation principle and the equation of state (macromodel). The pressure and the flow rate variation with respect to time are provided for several time-dependent configurations and the dependency of the results on the initial Knudsen number and pressure ratio as well as on the length of the tube is analyzed. The proposed methodology, which is applicable when the volume of the chambers is significantly larger than the volume of the tube, is valid in the whole range of the Knudsen number and computationally very efficient. © *2014 American Vacuum Society*.
[http://dx.doi.org/10.1116/1.4830283]

I. INTRODUCTION

Steady-state rarefied gas flows through tubes of variable length and cross section have attracted considerable attention over the years. In the case of long channels, the flow depends on the Knudsen number and the type of the cross section, and linearized kinetic model equations[1,2] have been applied with great success, providing accurate results with minimum computational effort.[3–12] In the case of channels of finite length, in addition to the above parameters, the pressure ratio and the length of the channel, as well as the end effects, are introduced in the investigation, increasing significantly the computational effort. However, both the direct simulation Monte Carlo (DSMC) method[13–17] and deterministic linear and nonlinear kinetic modeling[18–25] have been successfully applied to provide accurate results.

Time-dependent rarefied gas flows, despite their theoretical and practical importance, have received much less attention. Obviously, the involved computational effort is increased since the time dimension is added in the simulations. Applications where the implemented rarefied flow conditions are dynamically changing are very extensive and include processes in high energy and fusion facilities, space instrumentation, filtering, CD/DVD metallization, vacuum gauges, mass spectrometers, vacuum metrology, leak detection, MEMS, etc.

Recently, there is some effort in simulating time-dependent internal rarefied gas flows. The oscillatory slip flow[26] and the unsteady fully developed flow[27] in long channels have been modeled based on the Navier–Stokes equations subject to slip boundary conditions and the linearized Bhatnagar-Gross-Krook model equation,[28] respectively. In addition, based on the DSMC method, the transient flow of a rarefied gas through an orifice and a short tube has been simulated.[29,30] Also, the unsteady flow through a slit[31] has been modeled in a deterministic manner based on the nonlinear Shakhov model.[32]

In most of these cases, however, the flow configuration consists of two large reservoirs connected by a channel, and it is assumed that far from the channel inlet and outlet, the upstream and downstream conditions remain constant. The computational size of the upstream and downstream domains is taken large enough in order to justify this assumption, but still much smaller than the actual size of the reservoirs, while throughout the time evolution of the flow (including the final equilibrium state), the computational boundaries remain open, i.e., particles are moving in and out. The characteristic time is defined as the ratio of a characteristic distance (e.g., the radius of the orifice or the tube) over the most probable molecular velocity, and it has been found that in the case of short tubes the time needed to reach steady-state conditions varies approximately from few up to 50 μs.[29,30] This type of time-dependent flow is not easily detected and measured with the available instrumentation, where successive measurements may be done in time intervals of milliseconds.

Another time-dependent flow configuration, which likely is of more practical interest, is when the upstream and downstream pressures are changing with time. In this system, initially, the pressure in the upstream and downstream chambers is different, and then due to a valve opening, a time-dependent gas expansion from the high pressure chamber through the tube toward the low pressure chamber is evolved. During this process, which may be in the whole range of the Knudsen number, the pressure in the upstream chamber drops and in the downstream raises until they

[a)]Electronic mail: diva@uth.gr

become equal to each other, while the flow rate has a maximum value immediately after the valve opening and then is monotonically reduced. This time-dependent flow configuration is used in a recently built calibration facility where the response and relaxation times of vacuum gauges due to pressure changes are measured.[33,34]

It is important to note that modeling this flow configuration based solely on kinetic equations or DSMC simulations is computationally impractical mainly due to the size of the computational domain, which now must include the whole volume of the two chambers, in connection with the required very small time step. Reasonable arguments taking advantage of the specific characteristics of the flow must be drawn in order to introduce acceptable simplifications in modeling and greatly reduce the computational effort.

In this framework, very recently, based on the infinite capillary theory, a general approach has been introduced to model this time-dependent flow configuration in the case of the two chambers connected with a long tube.[35] The well-known methodology for establishing the steady-state mass flow rate and the pressure distribution in long channels[5–7] is extended to the case of unsteady flows, and a partial differential equation for the unknown transient pressure variation along the tube is deduced and numerically solved, based on numerical results obtained by the fully developed stationary kinetic equations. The results include the tube pressure variation in time and space as well as the pressure variation in the two chambers and are valid and accurate in the whole range of the Knudsen number. In this flow configuration, since the capillary is infinitely long, the volumes of the capillary and the chambers as well as the corresponding characteristic times are of the same order.

In the present work, we consider the same unsteady flow configuration where, however, the two chambers are connected with a tube of finite length. To model this flow, we introduce an alternative methodology, while certain issues of the above described approach are applied. Since now the volume of the tube is much smaller than the volume of the chambers, the evolution of the flow is modeled in a hybrid manner. At each time step, based on kinetic theory, a steady-state flow configuration is solved to estimate the amount of gas passing through the tube (micromodel), and then, the pressure of the two vessels is updated by applying the mass conservation principle and the equation of state (macromodel). Based on this approach, the variation of the pressure in the chambers and of the flow rate through the tube with respect to time is provided for several configurations. The dependency of the results on the initial reference Knudsen number and pressure ratio, as well as on the length of the tube is analyzed. It is noted that a hybrid methodology exploiting time scale separation has been also proposed for microactuators modeling.[36,37] The theoretical background and a detailed description on the advantages of such hybrid type simulations are given in a recent paper,[38] where several multiscale methodologies are analyzed.

II. STATEMENT OF THE PROBLEM

The system configuration that is examined is presented in Fig. 1 and includes two chambers connected by a tube of finite length L and radius R. The two chambers, denoted by A and B, have large but finite volumes V_A and V_B, respectively. The volume of the capillary is negligibly small compared to the volume of the chambers.

Initially, at time $t = 0$, the pressure and temperature in the two vessels are denoted by $P_i^{(0)}, T_i^{(0)}$, with $i = A, B$. The gas rarefaction, at time $t = 0$, in the two vessels is characterized by the initial Knudsen numbers defined as

$$Kn_i^{(0)} = \frac{\sqrt{\pi}}{2}\frac{\mu_i^{(0)} v_i^{(0)}}{P_i^{(0)} R}, \quad i = A, B,$$

where $\mu_i^{(0)}$ and $v_i^{(0)} = \sqrt{2R_g T_i^{(0)}}$, with R_g denoting the gas constant, are the viscosity and the most probable molecular velocity at temperature $T_i^{(0)}$.

Here, at time $t = 0$, we consider without loss of generality, $P_A^{(0)} > P_B^{(0)}$. Then, the valve in the inlet of the tube is rapidly opening, and the time-dependent gas expansion between the two finite volume vessels is evolved. During the process, the pressure in the upstream vessel A is reduced, while in the downstream vessel B is increased up to the point where the two pressures become equal to each other. In parallel, the

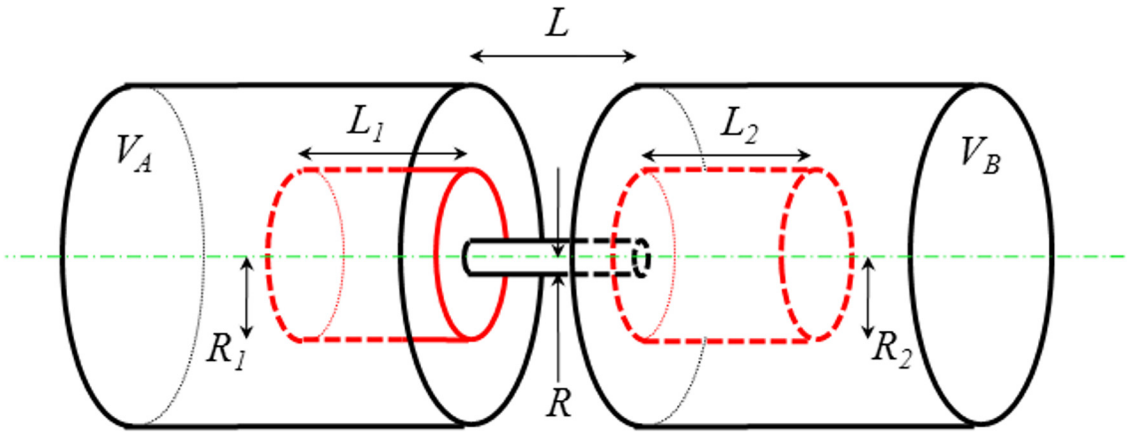

FIG. 1. (Color online) Schematic shown the system configuration consisting of the two chambers V_A, V_B with the connecting tube as well as the kinetic inlet and outlet computational domain.

mass flow rate $\dot{M}$ through the tube has its maximum value at the largest pressure difference immediately after the opening of the valve and then gradually is decreased as the pressure difference between the two vessels is reduced, and it finally becomes zero when the pressure difference is also equal to zero. The objective is to compute the pressure and temperature evolution $P_i(t)$ and $T_i(t)$, $i = A, B$ in the chambers, as well as the mass flow rate $\dot{M}(t)$ through the tube with respect to time for $t > 0$.

III. HYBRID MODELING

It is clear that processes in the chambers and in the tube are coupled. However, the volume of the tube is taken to be much smaller than the volume of the chambers, and as it will be shown in Sec. III A, the same applies for the corresponding characteristic times. These observations imply that the distance and the period over which the macroscopic quantities may vary are significantly smaller in the tube than those in the chambers. Thus, it is reasonable to exploit the space and time scale separation and to implement a hybrid model.[38] In particular, the evolution of the macroscopic quantities in the chambers at time $t + \Delta t$, where Δt is the macroscopic time step, are predicted by a simple macromodel where mass conservation is applied. The mass flow rate of the gas passing through the tube at time t has been computed by a micromodel, which is based on a suitable kinetic solver. An explicit-type coupling of the two models is applied, i.e., the micro and macromodels are applied successively (not simultaneously). The two models and their coupling process are described below.

A. Flow through the tube (micromodel)

At time t, based on the current upstream and downstream pressure and temperature, the rarefied gas flow through a tube of finite length L and radius R is simulated to compute the mass flow rate. The computational domain, shown in Fig. 1, consists of the tube plus the inlet and outlet cylindrical volumes adjacent to the tube ends, defined by (R_1, L_1) and (R_2, L_2). These volumes are large enough to ensure uniform conditions at the boundaries but much smaller than the volumes of chambers A and B. The case of purely pressure driven flow, i.e., when the temperature in the two chambers is the same, has been thoroughly studied via kinetic theory and numerical results in the whole range of the Knudsen number have been reported in the literature, based on both the DSMC method[14–17] and on deterministic kinetic modeling.[22,23,25] The dimensionless solution depends on three parameters, namely, the reference Knudsen number, the ratio of the downstream over the upstream pressure, and the ratio of the length over the radius of the tube. The case of flows driven both by pressure and temperature gradients have also been studied,[39–41] and the solution still depends on the same three parameters as before plus the temperature distribution along the tube wall and the ratio of the downstream over the upstream temperature which must be provided.

These parameters in the present notation are the Knudsen number

$$Kn_A = \frac{\sqrt{\pi}}{2}\frac{\mu_A \upsilon_A}{P_A R}, \tag{1}$$

with $\upsilon_A = \sqrt{2R_g T_A}$, the pressure and temperature ratios P_B/P_A and T_B/T_A, respectively, and the tube ratio L/R. Once these parameters are specified, the kinetic solver is applied at time t, to yield the dimensionless flow rate $W = W(Kn_A, P_B/P_A, T_B/T_A, L/R)$, which is connected to the mass flow rate $\dot{M}$ according to

$$W = \dot{M}/M_{\mathrm{fm}}, \tag{2}$$

where $M_{\mathrm{fm}} = R^2 P_A \sqrt{\pi}/\upsilon_A$ is the mass flow rate through an orifice at the free molecular limit.[5] Then, it is readily seen that

$$\dot{M} = W\frac{R^2 P_A \sqrt{\pi}}{\upsilon_A}. \tag{3}$$

The characteristic time of this flow is defined as the time needed to cross the tube radius with the most probable velocity, i.e.,

$$t_m = R/\upsilon_A^{(0)}. \tag{4}$$

Typical characteristic times are in the order of 10^{-6}s. It has been found that the time needed to establish steady-state conditions varies, depending on the flow parameters, approximately from 5 up to 50 characteristic times.[27,29,30] For example, in the case of helium flowing through a tube of a radius $R = 1$ mm, the characteristic time is about one microsecond, and then the total time to reach equilibrium, depending upon the length of the tube and the pressure ratio, is in the range from a few up to one hundred microseconds.

B. Temporal evolution of pressure in the chambers (macromodel)

By making a mass balance, the temporal evolution of the masses of the gas in the two chambers are defined by the ordinary differential equations as

$$\frac{dM_A}{dt} = -\frac{dM_B}{dt} = -\dot{M}(t), \tag{5}$$

where $M_A(t)$ and $M_B(t)$ is the mass of the gas at time t in the containers A and B, respectively, and $\dot{M}(t)$ is the mass flow rate of the gas moving in unit time from vessel A to B, estimated by the kinetic solver. By substituting in Eq. (5), the mass of the gas in each container according to the equation of state

$$P_i(t)V_i = M_i(t)R_g T_i(t), \quad i = A, B, \tag{6}$$

and the mass flow rate according to Eq. (3), the following ordinary differential equations, describing the pressure evolution in chambers A and B, respectively, are obtained:

$$\frac{dP_A}{dt} = -W(t)\frac{\sqrt{\pi}}{2}\frac{R^2}{V_A}P_A(t)\upsilon_A(t) + \frac{P_A(t)}{T_A(t)}\frac{dT_A}{dt}, \tag{7a}$$

$$\frac{dP_B}{dt} = W(t)\frac{\sqrt{\pi}}{2}\frac{R^2}{V_B}P_A(t)\frac{v_B^2(t)}{v_A(t)} + \frac{P_B(t)}{T_B(t)}\frac{dT_B}{dt}. \tag{7b}$$

The above ordinary difference equations with the initial conditions $P_A(0) = P_A^{(0)}$ and $P_B(0) = P_B^{(0)}$ describe the time evolution of the pressure in the upstream and downstream reservoirs. The dimensionless flow rate $W(t)$ is computed from the kinetic solver, while the temperature evolution must be given from a supplementary thermodynamic relation (e.g., isentropic processes in the chambers).

It is convenient to introduce the dimensionless quantities

$$p_A(t) = \frac{P_A(t)}{P_A^{(0)}}, \quad p_B(t) = \frac{P_B(t)}{P_A^{(0)}}, \quad \tau_A(t) = \frac{T_A(t)}{T_A^{(0)}},$$
$$\tau_B(t) = \frac{T_B(t)}{T_A^{(0)}}, \quad t^* = \frac{t}{t_M}, \tag{8}$$

where $P_A^{(0)}$ and $T_A^{(0)}$ are the reference pressure and temperature and

$$t_M = \frac{V_A/R^2}{v_A^{(0)}} \tag{9}$$

is the reference characteristic time. Equations (7) in dimensionless form, with the corresponding initial condition, are rewritten as

$$\frac{dp_A}{dt^*} = -\frac{\sqrt{\pi}}{2}W(t^*)\sqrt{\tau_A(t^*)}p_A(t^*) + \frac{p_A(t^*)}{\tau_A(t^*)}\frac{d\tau_A}{dt^*},$$
$$p_A(0) = 1, \tag{10a}$$

$$\frac{dp_B}{dt^*} = \frac{\sqrt{\pi}}{2}W(t^*)\frac{V_A}{V_B}\frac{\tau_B(t^*)}{\sqrt{\tau_A(t^*)}}p_A(t^*) + \frac{p_B(t^*)}{\tau_B(t^*)}\frac{d\tau_B}{dt^*},$$
$$p_B(0) = p_B^{(0)}/p_A^{(0)}. \tag{10b}$$

This set of equations does not depend on the type of the gas, while its dependency on the tube geometry is intrinsically introduced through W. Since $W(t^*)$ depends on the pressure, this is a set of two nonlinear ordinary differential equations, and it is solved numerically by a typical integration solver to compute the pressure temporal evolution in the two chambers. The proposed simple macromodel is valid provided that the assumption of uniform conditions in the chambers at each time step is justified.

C. Coupling

As it seen from the above description, the estimation of the dimensionless flow rate through the tube depends on the conditions in the chambers, while the estimation of the pressure in the chambers depends on the dimensionless flow rate and therefore the two models are coupled. However, the coupling of the two models in a fully implicit manner is computationally very expensive and impractical.

It is noted that in order to obtain kinetic results of acceptable error the numerical time step in the micromodel is about one hundred of the characteristic time, i.e., $\delta t = 0.01 \times t_m$, while the size of the inlet and outlet volumes must be defined approximately as $R_1 = L_1 = R_2 = L_2 = 8R$.[16,17,29,30] The involved overall CPU time, when the kinetic code is running on a single processor, depending on the flow parameters, is from several hours up to few days or weeks. It is clear that solving solely with the kinetic model the whole domain including the whole volume of chambers A and B, which may be several orders of magnitude larger than the computational domain implemented in the kinetic solver, is computationally a formidable task.

The ratio of the characteristic times of the macro over the micromodel, given by Eqs. (9) and (4) respectively, is

$$\frac{t_M}{t_m} = \frac{V_A}{R^3}. \tag{11}$$

Therefore, as long as the characteristic dimension of the chambers (e.g., a length equal to the cubic root of its volume) is one order of magnitude larger than the radius of the tube, the characteristic time in the chambers will be several orders of magnitude larger than the characteristic time in the tube. Then, when a change is induced, the microsystem relaxes to its equilibrium state much faster than the macrosystem and processes occurring at the microlevel are loosely coupled to the ones at the macrolevel. This means that the applied time and space scale separation between the two models as well as the quasisteady response of the micro to the macrostate are reasonable and will provide results of acceptable error.[38] In addition, the imposed parameters must allow the assumed uniform conditions in the chambers.

The hybrid model is simple and works as follows:

(1) At time t^* based on the input parameters $Kn_A(t^*)$, $p_B(t^*)/p_A(t^*)$, $\tau_B(t^*)/\tau_A(t^*)$, L/R the kinetic solver is applied to compute $W(t^*)$.
(2) Then, Eqs. (10) with a supplementary thermodynamic relation (discussed in Sec. IV) are solved to yield $p_i(t^* + \Delta t^*)$ and $\tau_i(t^* + \Delta t^*)$, $i = A, B$, with Δt^* denoting the dimensionless time step of the macromodel.
(3) The code is returning in step 1 and based on the updated chamber parameters, the flow rate $W(t^* + \Delta t^*)$ is computed. The marching scheme in time is continued until the equilibrium state is reached.

For the purposes of the present work, a dense kinetic database of stationary flow results has been constructed over a wide range of all input parameters. Based on this database, the hybrid model has been implemented for several flow configurations described in Sec. IV. Whenever is needed, an interpolation between the available data in the database is performed. In general, the present hybrid model, due to the proposed simple coupling process, is suitable in the cases of smooth variation of pressure in the upstream and downstream vessels. In the case of abrupt pressure changes, a more complex implicit-type coupling scheme will be needed to properly capture the dynamic behavior of the system.

IV. RESULTS AND DISCUSSION

The above methodology has been applied to simulate gas expansions assuming (1) isothermal and (2) isentropic conditions in the chambers. The dependency of the results on the initial pressure ratio, the initial Knudsen number, and the dimensionless tube length is analyzed. The evolution of the macroscopic quantities is predicted, and a parametric analysis is performed. Results are provided in dimensionless and dimensional form for the cases of $V_B \gg V_A$ and $V_B = V_A$.

A. Isothermal expansion

In this process, it is assumed that $T_A^{(0)} = T_B^{(0)}$ and that there is no temperature variation in the chambers with respect to time, i.e., $\tau_A(t^*) = \tau_B(t^*) = 1$. Then, the pressure evolution equations (10) are simplified to

$$\frac{dp_A}{dt^*} = -\frac{\sqrt{\pi}}{2} W(t^*) p_A(t^*), \quad p_A(0) = 1, \tag{12a}$$

$$\frac{dp_B}{dt^*} = \frac{\sqrt{\pi}}{2} W(t^*) \frac{V_A}{V_B} p_A(t^*), \quad p_B(0) = p_B^{(0)}/p_A^{(0)}, \tag{12b}$$

where $W(t^*)$ is obtained at each t^* from the kinetic solver modeling purely pressure driven stationary flow through a tube. The temporal evolution of the flow is simulated until the pressure difference between the two chambers is reduced to 1% of the initial pressure difference, i.e.,

$$(p_A - p_B)/(p_A^{(0)} - p_B^{(0)}) < 0.01. \tag{13}$$

The time at which condition (13) is fulfilled is called equilibrium time, and it is denoted by t_{eq}^*.

The case of $V_B \gg V_A$ is considered first. The dependency of the temporal evolution of $p_A(t^*)$ and $W(t^*)$ on the initial pressure ratio $p_B^{(0)}/p_A^{(0)}$, the initial Knudsen number $Kn_A^{(0)}$, and the tube dimensionless length L/R is shown in Figs. 2–4, respectively. In all cases, the $p_A(t^*)$ and $W(t^*)$ plots are starting at $t^* = 0$, where $p_A(0) = 1$ and $W(0)$ has its maximum value, and then both quantities are monotonically reduced until the simulation is concluded at time $t^* = t_{eq}^*$. It is noted that in the case of $V_B \gg V_A$, Eq. (10b) yields $p_B(t^*) = p_B(0) = p_B^{(0)}/p_A^{(0)}$, i.e., as expected, there is no pressure variation in the chamber B with respect to time.

In Fig. 2, the transient evolution of $p_A(t^*)$ and $W(t^*)$ is plotted for $p_B^{(0)}/p_A^{(0)} = [0, 0.1, 0.3, 0.5]$. It is seen that as the initial pressure ratio is decreased, i.e., the initial pressure difference is increased, the corresponding flow rates are also increased, and therefore the pressure gradient with respect to time is stiffer. The flow rate tends to zero as time is increased for all pressure ratios except $p_B^{(0)}/p_A^{(0)} = 0$, in which case it tends to the corresponding nonzero steady-state solution in the free molecular limit.[16] Also, as $p_B^{(0)}/p_A^{(0)}$ is decreased, the time t_{eq}^* to reach equilibrium is increased, which is due to the larger difference between the initial and equilibrium pressures.

The effect of the initial Knudsen number is shown in Fig. 3, where the $p_A(t^*)$ and $W(t^*)$ plots are given for $Kn_A^{(0)} = [0.01, 0.1, 1, \infty]$ and $p_B^{(0)}/p_A^{(0)} = [0, 0.1]$. It is seen that the effect of the initial degree of gas rarefaction on the temporal pressure evolution is negligible for $Kn_A^{(0)} \geq 1$ and it becomes more significant for $Kn_A^{(0)} < 1$. A similar behavior, probably not as strong for the large Knudsen numbers, is observed also for the flow rate evolution. For $p_B^{(0)}/p_A^{(0)} = 0$, as time is increased, the flow rates are approaching the corresponding

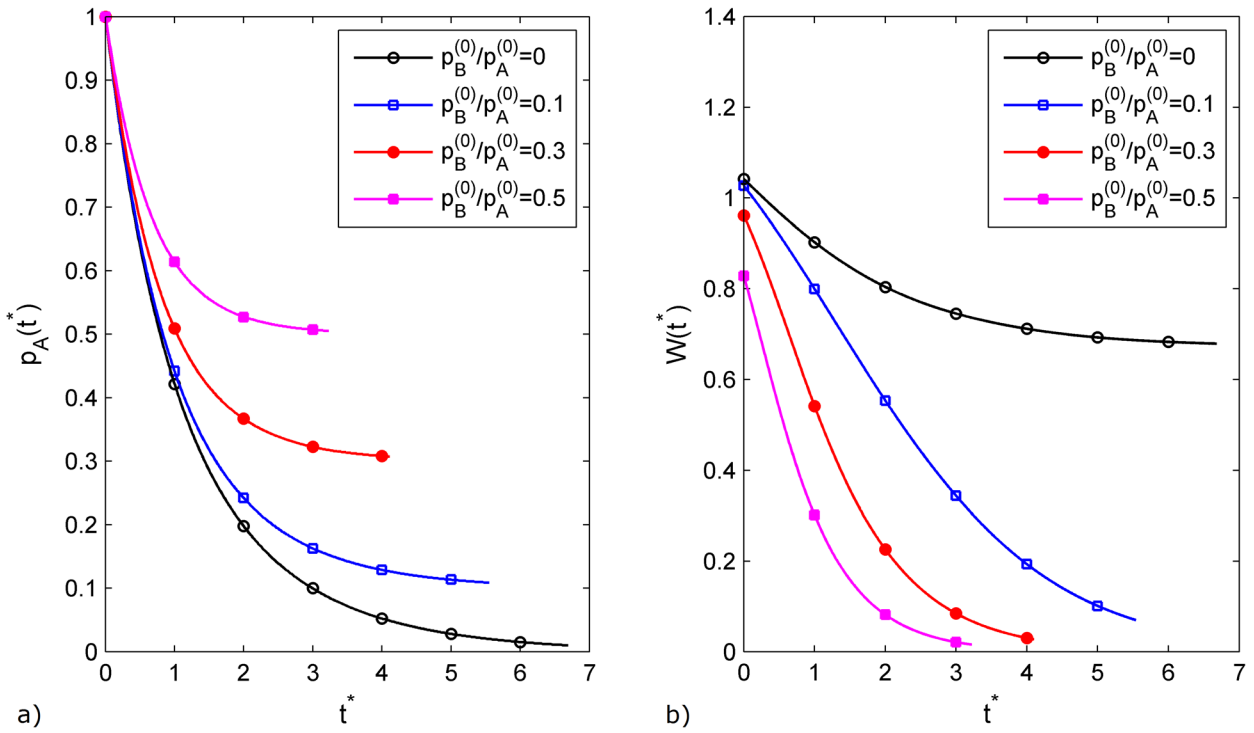

FIG. 2. (Color online) Temporal evolution of dimensionless (a) pressure $p_A(t^*)$ and (b) flow rate $W(t^*)$ for various values of the initial pressure ratio $p_B^{(0)}/p_A^{(0)}$ with initial Knudsen number $Kn_A^{(0)} = 0.1$ and $L/R = 1$.

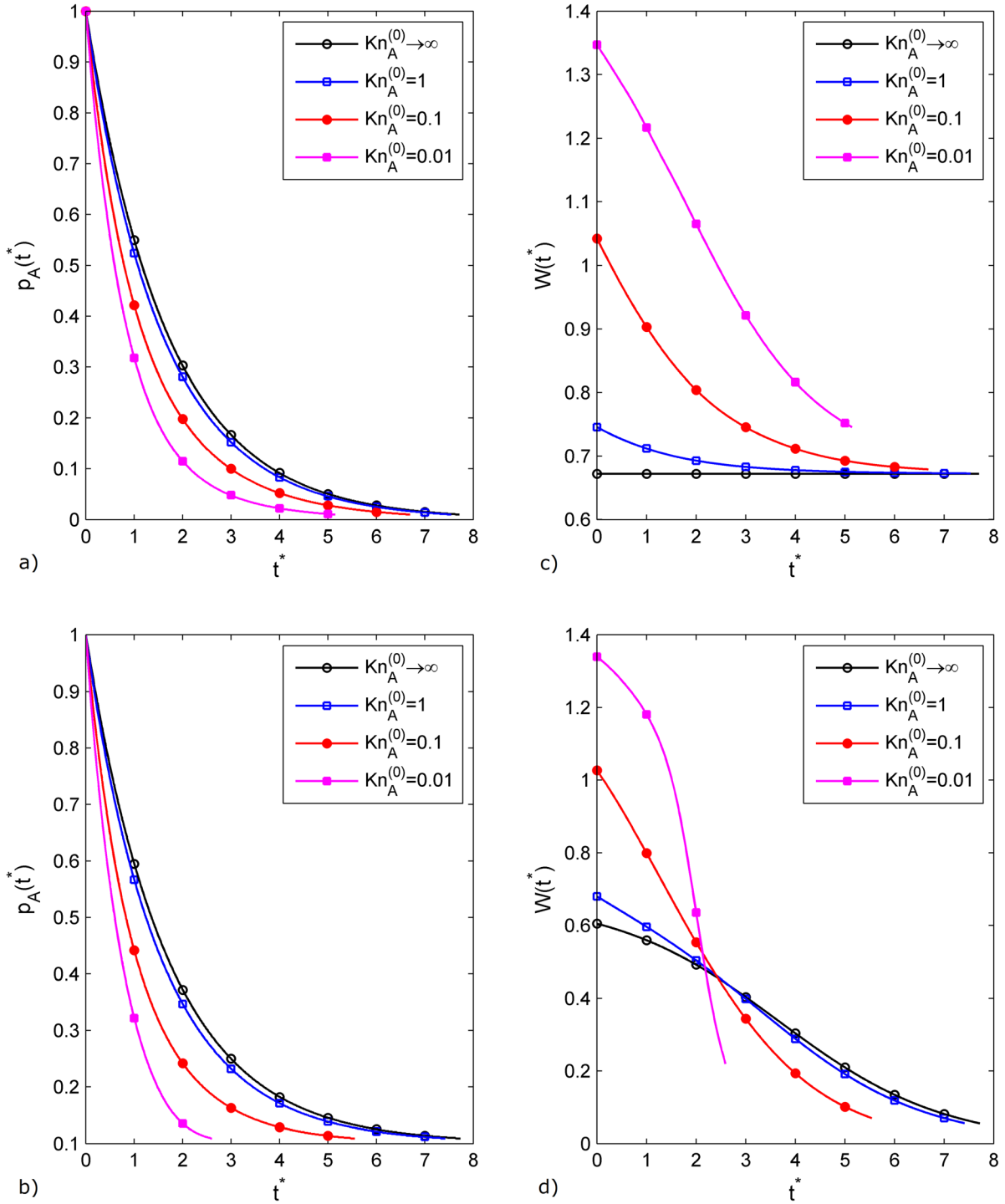

FIG. 3. (Color online) Temporal evolution of dimensionless pressure $p_A(t^*)$ with initial pressure ratio (a) $p_B^{(0)}/p_A^{(0)} = 0$ and (b) $p_B^{(0)}/p_A^{(0)} = 0.1$ and of dimensionless mass flow rate $W(t^*)$ with initial pressure ratio c) $p_B^{(0)}/p_A^{(0)} = 0$ and d) $p_B^{(0)}/p_A^{(0)} = 0.1$ for various values of the initial Knudsen number $Kn_A^{(0)}$ with $L/R = 1$.

nonzero steady-state solutions,[16] while for $p_B^{(0)}/p_A^{(0)} = 0.1$, they tend to zero. Comparing the results between $p_B^{(0)}/p_A^{(0)} = 0$ and 0.1, it is seen that the pressure plots are qualitatively similar, which is not the case for the flow rate plots. In the case of $p_B^{(0)}/p_A^{(0)} = 0$, the corresponding flow rates are always decreased as the initial Knudsen number is increased, while in the case of $p_B^{(0)}/p_A^{(0)} = 0.1$, this is true only for the first part of the transition period up to about 2.0–2.5 characteristic times t_M and then it is the other way around. However, this second part of the transition flow is not very important since both pressure and flow rate are close to their equilibrium values. The results of the flow rate for $p_B^{(0)}/p_A^{(0)} = 0.1$, shown in Fig. 3, are typical for the flow rates when the initial pressure ratio is different than zero. It is noted that the equilibrium time t_{eq}^* is increased as $Kn_A^{(0)}$ is increased, i.e., more rarefied flows require more time to

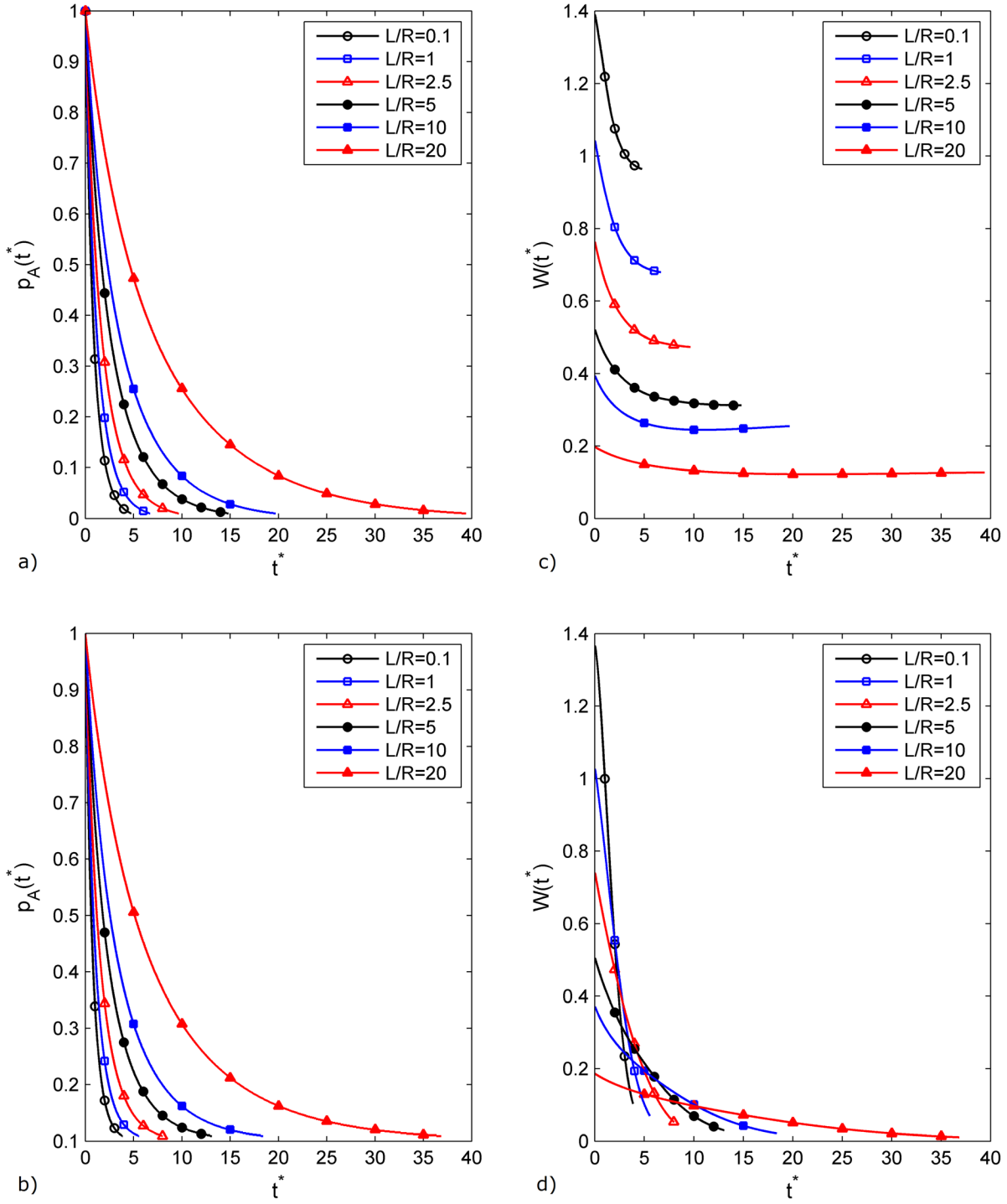

FIG. 4. (Color online) Temporal evolution of dimensionless pressure $p_A(t^*)$ with initial pressure ratio (a) $p_B^{(0)}/p_A^{(0)} = 0$ and (b) $p_B^{(0)}/p_A^{(0)} = 0.1$ and of dimensionless mass flow rate $W(t^*)$ with initial pressure ratio (c) $p_B^{(0)}/p_A^{(0)} = 0$ and (d) $p_B^{(0)}/p_A^{(0)} = 0.1$ for various values of L/R with initial Knudsen number $Kn_A^{(0)} = 0.1$.

reach equilibrium. This is due to the fact that, in general, the flow rate is reduced as the gas rarefaction is increased.

Next, the dependency of the flow on the dimensionless tube length is shown in Fig. 4, where $p_A(t^*)$ and $W(t^*)$ are plotted for $L/R = [0.1, 1, 2.5, 5, 10, 20]$ and $p_B^{(0)}/p_A^{(0)} = [0, 0.1]$. In all cases, as the tube length is decreased, the pressure gradient with respect to time is increased, since the flow rate becomes faster. Also, the time t_{eq}^* to reach equilibrium is increased as the tube length is increased, since in longer tubes the flow speed is decreased and more time is needed to reach equilibrium. It is noted that the flow rates $W(t^*)$ are computed based on DSMC and deterministic nonlinear kinetic modeling for $L/R \leq 5$, while for $L/R = [10, 20]$ linear fully developed kinetic modeling is implemented.

The case of having two chambers of about the same volume is considered next by taking $V_B = V_A$. In this case, there is pressure variation in both chambers. Equations (12) are solved to deduce the temporal evolution of $p_A(t^*)$, $p_B(t^*)$,

and $W(t^*)$. Indicative results are presented in Fig. 5 for various values of the initial Knudsen number $Kn_A^{(0)}$ with $p_B^{(0)}/p_A^{(0)} = 0$ and $L/R = 1$. It is seen that the pressure decrease in chamber A is symmetric with the pressure increase in chamber B. The symmetry axis is located at $p_A(t^*) = 0.5$. Beyond that the dependency of the pressure and flow rate time variation on the initial Knudsen number as well as on the other parameters is qualitatively the same with the case of $V_B \gg V_A$. Of course when $V_B = V_A$ the required equilibrium time t_{eq}^* is reduced compared to the corresponding one, when $V_B \gg V_A$.

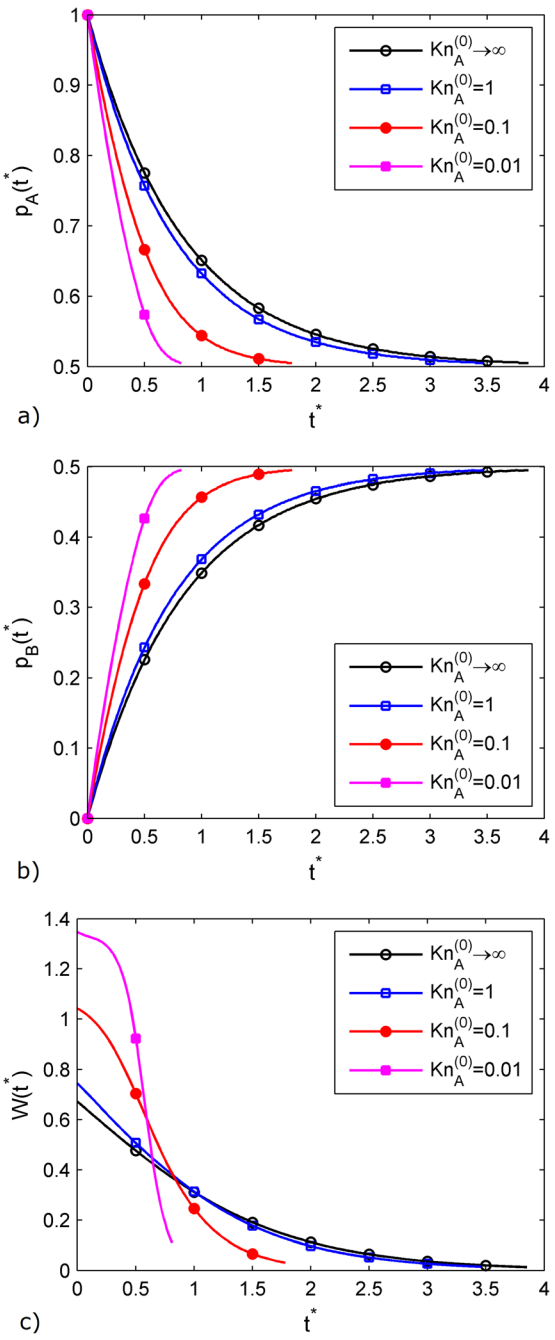

FIG. 5. (Color online) Temporal evolution of dimensionless (a) upstream pressure $p_A(t^*)$, (b) downstream pressure $p_B(t^*)$, and (c) flow rate $W(t^*)$ for various values of the initial Knudsen number $Kn_A^{(0)}$ with $L/R = 1$ and initial pressure ratio $p_B^{(0)}/p_A^{(0)} = 0$.

To have a more detailed view of the equilibrium time t_{eq}^*, which is a quantity of main importance, tabulated results are provided in Tables I and II for $V_B \gg V_A$ and $V_B = V_A$, respectively, in a wide range of all involved parameters. It is seen that t_{eq}^* is increased as L/R is increased as well as the initial pressure difference is increased (or $p_B^{(0)}/p_A^{(0)}$ is decreased). With regard to the initial Knudsen number it is seen that for $L/R \leq 5$ as $Kn_A^{(0)}$ is increased, t_{eq}^* is also increased, while for $L/R = 20$, t_{eq}^* has a maximum at $Kn_A^{(0)} = 1$. It is believed that this is due to the so-called Knudsen minimum, where in the case of long channels there is a minimum dimensionless flow rate at $Kn \approx 1$. The above observations are valid both for $V_B \gg V_A$ and $V_B = V_A$. Roughly speaking, in the latter case, the computed t_{eq}^* are about half of the corresponding ones in the former case.

B. Isentropic expansion

In this process the temperature changes of the gas in the two chambers are determined by the isentropic condition

$$\frac{T_i(t)}{T_i^{(0)}} = \left(\frac{P_i(t)}{P_i^{(0)}}\right)^{1-1/\gamma}, \quad i = A, B, \tag{14}$$

where γ is the heat capacity ratio of the gas. Initially, it is assumed that $T_A^{(0)} = T_B^{(0)}$. The corresponding expressions in dimensionless form are

$$\tau_i = p_i^{1-1/\gamma}, \quad i = A, B \tag{15}$$

with $\tau_i(0) = 1$ and by taking the time derivative it is easily deduced that

$$\frac{p_i(t^*)}{\tau_i(t^*)}\frac{d\tau_i}{dt^*} = \frac{\gamma - 1}{\gamma}\frac{dp_i}{dt^*}, \quad i = A, B. \tag{16}$$

TABLE I. Dimensionless equilibrium time t_{eq}^* in a wide range of flow parameters when $V_B \gg V_A$.

		L/R				
$Kn_A^{(0)}$	$p_B^{(0)}/p_A^{(0)}$	0.1	1	2.5	5	20
∞	0	5.43	7.71	11.1	16.7	39.0
	0.1	5.44	7.73	11.1	16.8	39.0
	0.3	5.42	7.76	10.9	16.8	39.0
	0.5	5.40	7.77	10.8	16.8	39.0
1	0	5.30	7.54	10.9	16.5	40.9
	0.1	5.19	7.42	10.7	16.5	42.0
	0.3	5.00	7.19	10.2	15.9	42.5
	0.5	4.76	6.89	9.68	15.0	42.2
0.1	0	4.73	6.69	9.66	14.8	39.4
	0.1	3.85	5.55	8.00	13.1	36.8
	0.3	2.81	4.11	6.34	9.88	30.1
	0.5	2.12	3.23	5.03	8.29	25.2
0.01	0	3.89	5.15	7.01	10.1	25.3
	0.1	2.08	2.60	3.51	4.92	12.5
	0.3	1.38	1.59	1.88	2.69	6.47
	0.5	1.09	1.22	1.42	1.90	4.43

TABLE II. Dimensionless equilibrium time t^*_{eq} in a wide range of flow parameters when $V_B = V_A$.

		L/R				
$Kn_A^{(0)}$	$p_B^{(0)}/p_A^{(0)}$	0.1	1	2.5	5	20
∞	0	2.70	3.87	5.45	8.38	19.5
	0.1	2.70	3.87	5.44	8.39	19.5
	0.3	2.70	3.88	5.42	8.39	19.5
	0.5	2.69	3.88	5.38	8.39	19.5
1	0	2.40	3.47	4.93	7.63	21.2
	0.1	2.37	3.43	4.86	7.53	21.1
	0.3	2.30	3.35	4.71	7.37	21.0
	0.5	2.24	3.27	4.53	7.26	20.8
0.1	0	1.22	1.79	2.73	4.41	13.2
	0.1	1.13	1.67	2.56	4.20	12.6
	0.3	0.982	1.46	2.29	3.82	11.5
	0.5	0.859	1.29	2.08	3.48	10.6
0.01	0	0.742	0.833	0.960	1.234	2.40
	0.1	0.686	0.765	0.884	1.122	2.20
	0.3	0.593	0.652	0.758	0.943	1.88
	0.5	0.518	0.564	0.661	0.810	1.64

Then, Eqs. (10), for the case of isentropic expansion, are reduced to

$$\frac{dp_A}{dt^*} = -\gamma\frac{\sqrt{\pi}}{2}W(t^*)\sqrt{\tau_A(t^*)}p_A(t^*), \quad p_A(0) = 1, \tag{17a}$$

$$\frac{dp_B}{dt^*} = \gamma\frac{\sqrt{\pi}}{2}W(t^*)\frac{V_A}{V_B}\frac{\tau_B(t^*)}{\sqrt{\tau_A(t^*)}}p_A(t^*), \quad p_B(0) = p_B^{(0)}/p_A^{(0)}. \tag{17b}$$

Results are provided for the case of $V_B \gg V_A$ and $p_B^{(0)}/p_A^{(0)} = 0$. The temporal evolution of dimensionless pressure $p_A(t^*)$, temperature $\tau_A(t^*)$, and flow rate $W(t^*)$ for various values of the initial Knudsen number $Kn_A^{(0)}$, with $L/R = 1$, are shown in Fig. 6. At each time step, the pressure and temperature are obtained from Eqs. (17a) and (15), respectively, while the flow rate from the kinetic solver. The corresponding equilibrium times are tabulated in Table III. In all cases, monatomic gases are considered, and thus, $\gamma = 5/3$. In general, the dependency of pressure and flow rate variation with respect to time is similar to the case of isothermal flow, while t^*_{eq} in the isentropic process is slightly smaller than the corresponding one in the isothermal process. The presented results are indicative for other initial pressure ratios and dimensionless tube lengths.

As it is stated before, in the case of $V_B \gg V_A$, there is no pressure variation in the chamber B with respect to time and then from Eq. (15) it is readily deduced that there is no temperature variation as well and the flow is driven purely due to the pressure difference. In contrary, in the case of $V_B = V_A$, there is a pressure and then a temperature variation according to Eq. (15) in chamber B. As a result, the temperature at each time step in the two chambers will be different, and in addition to the pressure driven flow, there is a temperature driven flow, well known as thermal creep flow. A

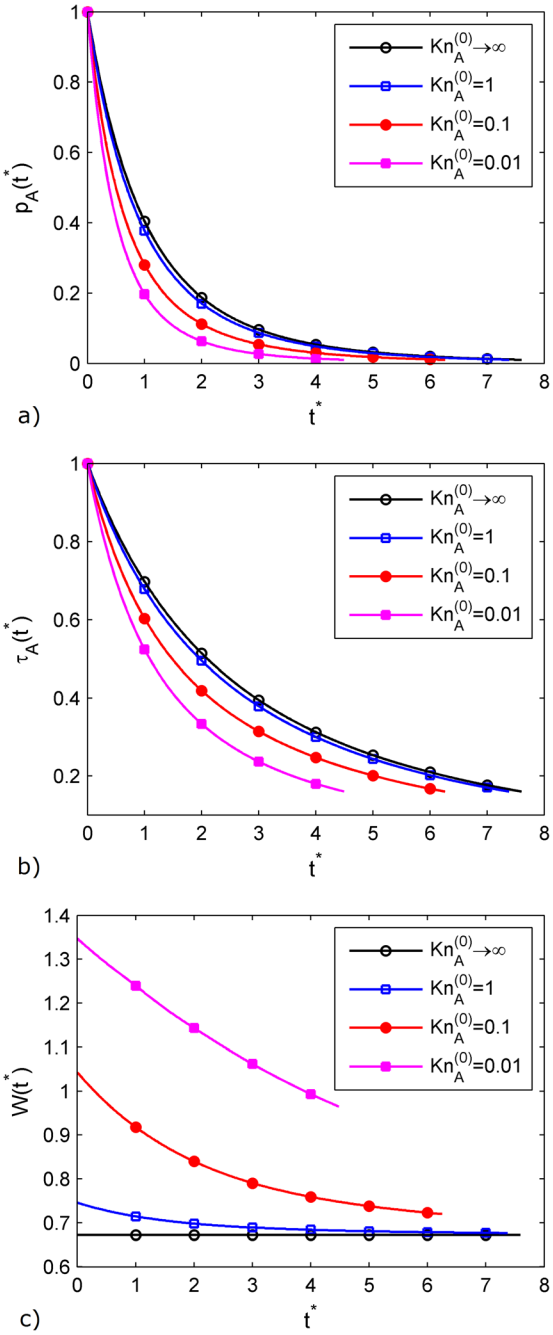

FIG. 6. (Color online) Temporal evolution of dimensionless (a) pressure $p_A(t^*)$, (b) temperature $\tau_A(t^*)$, and (c) flow rate $W(t^*)$ in the isentropic expansion for various values of the initial Knudsen number $Kn_A^{(0)}$ with $L/R = 1$ and initial pressure ratio $p_B^{(0)}/p_A^{(0)} = 0$ in the case of $V_B \gg V_A$.

TABLE III. Dimensionless equilibrium time t^*_{eq} of isentropic expansion into vacuum ($V_B \gg V_A$, $p_B^{(0)}/p_A^{(0)} = 0$).

	L/R			
$Kn_A^{(0)}$	0.1	1	2.5	5
∞	5.36	7.61	10.9	16.5
1	5.19	7.39	10.6	16.2
0.1	4.43	6.27	9.07	14.0
0.01	3.55	4.50	5.86	7.99

suitable kinetic solver, as the one described in the paper,[41] must be implemented to accurately estimate at each time step the flow rate W.

C. Isothermal and isentropic expansion of helium and xenon

Concluding this section, some dimensional results are provided for two monatomic gases, namely, helium (He) and xenon (Xe). These gases, having molecular molar masses $m_{\mathrm{He}} = 4.0026$ g/mol and $m_{\mathrm{Xe}} = 131.30$ g/mol, are representative in order to distinguish the different flow characteristics between light and heavy gases. In all cases presented here, the volume of chamber A is $V_A = 3$ L, the initial upstream pressure is $P_A^{(0)} = \left[0.1, 1, 10, 10^2, 10^3\right]$ Pa, and the gas is flowing through a tube of $L = R = 0.5$ mm into vacuum ($P_B^{(0)} = P_B = 0$). Since the two gases have different molecular masses the corresponding initial Knudsen numbers $Kn_A^{(0)}$ for helium and xenon are different. Initially, the temperatures are taken to be $T_A^{(0)} = T_B^{(0)} = 293$ K.

Based on Eq. (4), the characteristic microtime t_m for He and Xe are 0.45×10^{-6}s and 2.6×10^{-6}s, respectively, while based on Eq. (9) the corresponding characteristic macrotime t_M is 10.9 s and 62.3 s. The ratio of t_M over t_m is about 24×10^6. The sizes of the chambers and the tube have been chosen such that to match the ones of an experimental set up which is under way with the objective to perform time-dependent gas expansion measurements in the short future. In parallel, the provided results are indicative for related geometries.

In Table IV, the equilibrium time t_{eq}^* is tabulated for the case of isothermal conditions in the chambers. In the first column, the initial pressures $P_A^{(0)}$ are provided, followed by the initial Knudsen numbers $Kn_{A,\mathrm{He}}^{(0)}$ and $Kn_{A,\mathrm{Xe}}^{(0)}$ in columns two and three. In columns four and five, the equilibrium times are given for He and Xe, respectively, for the case of $V_B \gg V_A$ and the corresponding ones in the last two columns in the case of $V_B = V_A$.

It is seen that with the initial pressure varying from 0.1 to 10^3 Pa, the initial Knudsen numbers are in the whole range of gas rarefaction, varying from the viscous down to the free molecular regime, with the initial Knudsen numbers of He to be much higher than the corresponding ones of Xe. In both gases, as the initial pressure is reduced and the Knudsen number is increased, i.e., the gas rarefaction is increased, the values of the equilibrium times are increased.

TABLE IV. Equilibrium time t_{eq} in seconds for He and Xe and various values of the initial pressure $P_A^{(0)}$ in the case of isothermal expansion ($L = R = 0.5$ mm).

			$V_B \gg V_A = 3$L		$V_B = V_A = 3$L	
$P_A^{(0)}$ (Pa)	$Kn_{A,\mathrm{He}}^{(0)}$	$Kn_{A,\mathrm{Xe}}^{(0)}$	He	Xe	He	Xe
10^3	0.038	0.0075	66.0	308.6	12.0	49.2
10^2	0.38	0.075	79.4	405.6	31.7	95.6
10	3.8	0.75	83.4	466.0	41.1	207.3
1	38	7.5	83.8	478.7	42.0	238.3
10^{-1}	380	75	83.8	480.1	42.1	240.4

TABLE V. Equilibrium time t_{eq} in seconds for He and Xe and various values of the initial pressure $P_A^{(0)}$ in the case of isentropic expansion into vacuum with $V_B \gg V_A$ ($L = R = 0.5$mm).

$P_A^{(0)}$ (Pa)	$Kn_{A,\mathrm{He}}^{(0)}$	$Kn_{A,\mathrm{Xe}}^{(0)}$	He	Xe
10^3	0.038	0.0075	59.5	269.9
10^2	0.38	0.075	77.0	376.0
10	3.8	0.75	82.1	455.5
1	38	7.5	82.7	472.3
10^{-1}	380	75	82.7	473.7

This has been also observed in the dimensionless results. Here, it is seen that the time needed to reach steady-state conditions in the case of Xe is much larger than that of He. In particular, it is seen that t_{eq}^* for Xe is about three to six times larger than the corresponding one for He. This is attributed to the corresponding initial Knudsen numbers which are much smaller for He making the flow conditions more rarefied.

The equilibrium times for the case of isentropic conditions in the chambers with $V_B \gg V_A$ and the same parameters both for He and Xe are provided in Table V. Comparing these results with the corresponding ones in Table IV, it is seen that in high initial pressures, t_{eq}^* is smaller when the conditions in the chambers vary according to the isentropic law. However, for smaller initial pressures, i.e., in more rarefied conditions, the equilibrium times for both isothermal and isentropic processes are very close.

V. CONCLUSION

A hybrid model is implemented to investigate the time-dependent gas expansion from a high pressure chamber through a tube toward a low pressure chamber under rarefied conditions. Since in many occasions the volume of the chambers is much larger than that in tube a space and time scale separation is introduced. At each time step, a microstationary kinetic model computes the flow rate through the tube and then a simple macromodel based on the mass conservation principal provides the updated pressure and temperature in the chambers. The error introduced by the quasistate response of the micro to the macrostate is acceptable since the time needed for the microsystem to relax is several orders of magnitude smaller than the relaxing time of the macromodel.

The temporal evolution of pressure and temperature in the chambers, as well as of the mass flow rate through the tube up to the point where the system is very close to equilibrium is computed and analyzed. It has been found that the time t_{eq}^* needed to reach the stationary state is increased as the length of the tube and the initial pressure difference between the chambers are increased. Also, as the initial gas rarefaction is increased, the equilibrium time is monotonically increased when the dimensionless tube length is $L/R \leq 5$, while for $L/R \geq 10$, it appears a maximum for Knudsen number equal to one, which is related to the so-called Knudsen minimum in the case of long tubes. In

addition, the provided dimensional results clearly indicate that for the same tube length, initial pressure and initial pressure difference, t^*_{eq} is increased as the molecular mass of the gas is increased.

It is hoped that the present work will be helpful in the design and optimization of the dynamic response of vacuum gauges and other processes in various devices. A comparison of the present numerical results with measurements will be very useful and it is planned to be performed in the short future in a calibration facility at PTB. It is also planned to introduce more advanced coupling between the micro and macromodels in order to further improve the efficiency and applicability of the whole approach.

ACKNOWLEDGMENTS

Support through the EMRP IND12 project is gratefully acknowledged. The EMRP is jointly funded by the EMRP participating countries within EURAMET and the European Union.

[1]J. H. Ferziger and H. G. Kaper, *Mathematical Theory of Transport Processes in Gases* (North-Holland, Amsterdam, 1972).
[2]C. Cercignani, *The Boltzmann Equation and Its Application* (Springer, New York, 1988).
[3]K. Aoki, in *Rarefied Gas Dynamics*, edited by E. P. Muntz, D. P. Weaver, and D. H. Campbell (AIAA, Washington, DC, 1989), Vol. 118, 297 pp.
[4]Y. M. Shakhov, Comp. Math. Math. Phys. **36**, 1123 (1996).
[5]F. Sharipov and V. Seleznev, J. Phys. Chem. Ref. Data **27**, 657 (1998).
[6]F. Sharipov and V. Seleznev, J. Vac. Sci. Technol. A **12**, 2933 (1994).
[7]F. Sharipov, J. Vac. Sci. Technol. A **17**, 3062 (1999).
[8]D. Valougeorgis, Phys. Fluids **19**, 091702 (2007).
[9]I. Graur and F. Sharipov, Eur. J. Mech. B **27**, 335 (2007).
[10]G. Breyiannis, S. Varoutis, and D. Valougeorgis, Eur. J. Mech. B **27**, 609 (2008).
[11]S. Naris and D. Valougeorgis, Eur. J. Mech. B **27**, 810 (2008).
[12]S. Varoutis, S. Naris, V. Hauer, C. Day, and D. Valougeorgis, J. Vac. Sci. Technol. A **27**, 89 (2009).
[13]G. A. Bird, *Molecular Gas Dynamics and the Direct Simulation of Gas Flows* (Oxford University Press, Oxford, 1994).
[14]F. Sharipov, J. Fluid Mech. **518**, 35 (2004).
[15]T. Lilly, S. Gimelshein, A. Ketsdever, and G. N. Markelov, Phys. Fluids **18**, 093601 (2006).
[16]S. Varoutis, O. Sazhin, D. Valougeorgis, and F. Sharipov, J. Vac. Sci. Technol. A **26**, 228 (2008).
[17]S. Varoutis, D. Valougeorgis, and F. Sharipov, J. Vac. Sci. Technol. A **27**, 1377 (2009).
[18]V. V. Aristov, *Direct Methods for Solving the Boltzmann Equation and Study of Non-Equilibrium Flows* (Kluwer Academic, Dordrecht, 2001).
[19]A. Frezzotti, G. P. Ghiroldi, and L. Gibelli, Comput. Fluids **50**, 136 (2011).
[20]A. Frezzotti, G. P. Ghiroldi, and L. Gibelli, Comput. Phys. Commun. **182**, 2445 (2011).
[21]V. A. Titarev and E. M. Shakhov, Vacuum **86**, 1709 (2012).
[22]V. A. Titarev, J. Comput. Phys. **231**, 109 (2012).
[23]S. Pantazis and D. Valougeorgis, Eur. J. Mech. B **38**, 114 (2013).
[24]S. Pantazis, D. Valougeorgis, and F. Sharipov, Vacuum **26**, 26 (2013).
[25]V. A. Titarev, Vacuum **94**, 92 (2013).
[26]S. Colin, C. Aubert, and R. Caen, Eur. J. Mech. B **17**, 79 (1998).
[27]J. Lihnaropoulos and D. Valougeorgis, Fusion Eng. Des. **86**, 2139 (2011).
[28]P. L. Bhatnagar, E. P. Gross, and M. A. Krook, Phys. Rev. **94**, 511 (1954).
[29]F. Sharipov, J. Vac. Sci. Technol. A **30**, 021602 (2012).
[30]F. Sharipov, Vacuum **90**, 25 (2013).
[31]A. Polikarpov and I. Graur, Vacuum **101**, 79 (2014).
[32]E. M. Shakhov, Fluid Dyn. **3**, 95 (1968).
[33]K. Sonderegger, M. Dur, J. Buthig, S. Pantazis, and K. Jousten J. Vac. Sci. Technol. A **31**, 060601, 2013.
[34]K. Jousten, S. Pantazis, J. Buthig, R. Model, M. Wuest, and J. Iwicki, Vacuum **100**, 14 (2014).
[35]F. Sharipov and I. Graur, Vacuum **100**, 22 (2014).
[36]M. Ota, Y. He, and S. K. Stefanov, AIP Conf. Proc. 1134 (2007).
[37]Y. He, S. K. Stefanov, and M. Ota, AIP Conf. Proc. **1084**, 281 (2008).
[38]D. A. Lockerby, C. A. Duque-Daza, M. K. Borg, and J. M. Reese, J. Comput. Phys. **237**, 344 (2013).
[39]A. A. Alexeenko, S. F. Gimelshein, E. P. Muntz, and A. D. Ketsdever, Int. J. Therm. Sci. **45**, 1045 (2006).
[40]Yu. A. Anikin, O. I. Dodulad, Yu. Yu. Kloss, D. V. Martynov, P. V. Shuvalov, and F. G. Tcheremissine, Vacuum **86**, 1770 (2012).
[41]S. Pantazis, S. Naris, C. Tantos, D. Valougeorgis, J. Andre, F. Millet, and J. P. Perin, Fusion Eng. Des. **88**, 2384 (2013).